Oral presentation at
Workshop on HTS Josephson Junctions
and 3-Terminal Devices
Univ. of Twente
Enschede, The Netherlands
May 2-4, 1994

A Method For Increasing The I_cR_n Products In YBCO/Au/YBCO Junctions

Z.W. Dong, P. Hadley, R. Besseling and J. E. Mooij

Department of Applied Physics, Delft University of Technology Lorentzweg 1, 2628 CJ Delft, The Netherlands

We have developed a method for eliminating the excess conductance in YBCO/Au/YBCO step edge junctions. This fabrication procedure results in I_cR_n products of 7.8 mV at 4.2 K and 0.18 mV at 77 K. Using these junctions, we have fabricated SQUIDs with a flux noise of 3×10^{-5} Φ_o/\sqrt{Hz} at 77 K, with a 1/f noise knee at 1 Hz. Noise measurements were performed on SQUIDs in an open loop mode. Underdamped junctions can also be made with this fabrication technique. This may allow for the fabrication of relaxation oscillation SQUIDs operating at 77 K.

1. Introduction

One type of high T_c Josephson junctions that has exhibited low noise in SQUIDs are the SNS (YBCO/Au/YBCO) step edge junctions. I One undesirable feature of the standard fabrication procedure for these junctions is that the gold covers large areas of the YBCO electrodes. This creates an unnecessarily large shunt conductance that reduces the I_n product in these junctions. The excess conductance can be reduced without affecting the critical current by etching the excess gold away.² We have developed an alternative method for eliminating this excess conductance. An insulating layer is deposited between the YBCO and the Au. This fabrication procedure results in a dramatic improvement in the I_cR_n product (7.8 mV at 4.2 K and 0.18 mV at 77 K). The high $I_c R_n$ product translates into improved device performance. Using these junctions, we have fabricated SQUIDs with a flux noise of $3\times10^{-5} \Phi \sqrt{\sqrt{Hz}}$ at 77 K, with a 1/f noise knee at 1 Hz.

In this paper two types of junctions will be described. One is the standard YBCO/Au/YBCO step edge junctions (type A), and the other is the YBCO/Au/YBCO junctions with the insulating layer to reduce the shunt conductance (type B). Schematic drawings of these two junction types are shown in Fig. 1. In addition to higher I_cR_n products, it is possible to make the type B junctions underdamped. This means that the junctions have a hysteretic current-voltage characteristic. Underdamped junctions are essential for certain applications such as high- T_c relaxation oscillation SQUIDs (ROS).

2. Fabrication

The YBCO/Au/YBCO step edge junctions and dc-SQUIDs were fabricated by pulsed laser ablation using an entirely in-situ process.³ To fabricate the type A junctions, steps 300 - 400 nm deep were etched in an [001] LaAlO₃ or [001] MgO substrate by Ar ion

milling using a metal mask. In order to get a clean surface, we continued to etch with a low ion energy 10 minutes after the metal mask has been etched through. This process results in a step with about a 55° angle. The YBCO was then ablated at an angle of +30° so that a shadow gap was formed at the step. The thickness of the YBCO layer was typically half that of the step. The film is c-axis oriented, with a zero resistance transition temperature of 88 - 92 K and a critical current density at 77 K above 106 A/cm². The cross-sectional TEM. EDAX and the electrical R-T measurements showed that there was no YBCO film connection over the steps.³ Finally, a 200-300 nm thick Au film was ablated at another angle -30° on top of YBCO without breaking vacuum. A similar fabrication procedure is followed to make the type B junctions. The only difference is that a 50 - 100 nm thick SrTiO₃ layer is deposited on the YBCO at an angle of +30° before the Au is deposited.

Six dc-SQUIDs and fourteen junctions with widths of $3 \mu m$, $5 \mu m$, $10 \mu m$, $15 \mu m$, $20 \mu m$, $30 \mu m$, and $50 \mu m$ are fabricated on each chip using standard photolithography and ion-beam etching. The total time to fabricate these high- T_c devices using the *in-situ* technique was several hours and the yield of working devices was above 90 %.

3. Junction Characterization

The junctions could be well described by the RSJ model with thermal noise. The current-voltage characteristic at 77 K and 80 K for the type A and type B junctions are shown in Fig. 2. For the type A junctions, there is no hysteresis. At high temperature a thermal noise rounding occurs in the low voltage regime. The noise parameter, $\gamma = \hbar I_c J(ek_B T)$, is in the range 10 - 120 at 77 K for a 3-, 5-, 10- μ m-wide junctions. For both types of junctions, the critical current was about the same (20 - 345 μ A at 77 K for $w = 3 \sim 50 \mu$ m, $J_c \sim 5 \times 10^3$

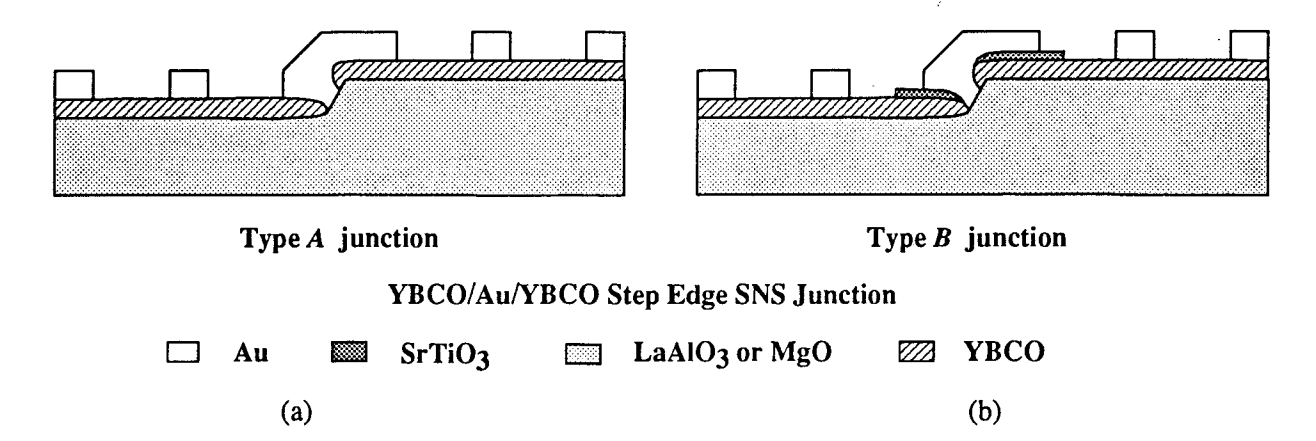


Fig. 1. Schematic drawings of two types of YBCO/Au/YBCO step-edge SNS junctions (a) nonhysteretic type A junction (b) hysteretic type B junction.

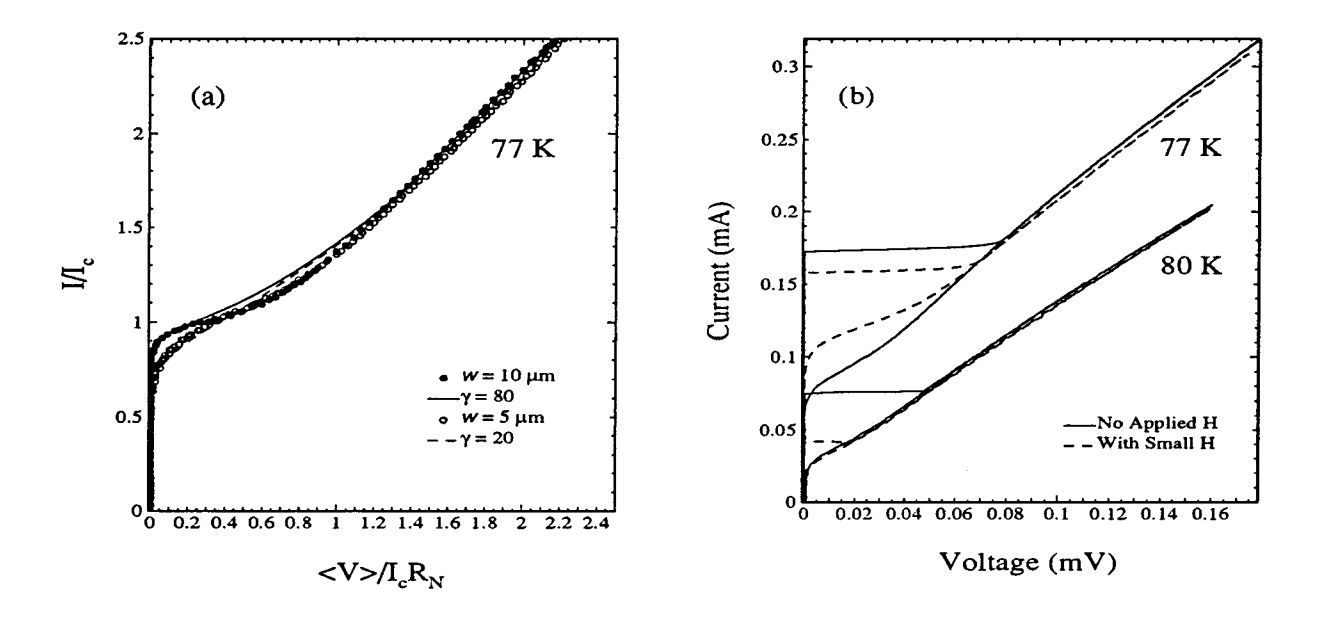


Fig. 2. (a) The current-voltage characteristics of type A junctions at 77 K. There is a thermal noise rounding in the small voltage regime. The points are the experimental data of junctions with w = 5, 10 μ m, and the curves are the simulations based on RSJ model with different thermal barrier height. (b) The hysteretic I-V curves from one of the type B junctions ($w = 10 \mu$ m) at 77 K and 80 K. The solid curve is without applying magnetic field and the dash curve is with applying a small magnetic field. From simulations based on the RSCJ model we estimate β_c to be 20.

A/cm²) and the R_n was nearly temperature independent. The resistance of the type B junctions was about 15 times greater than that of the type A junctions. If we assume that the effective area of the junction is the film thickness times the patterned width of the junction then the contact resistance for the type B junctions is $2 - 12 \Omega - \mu m^2$. This value is close to the values reported by Ekin et al.⁴ for clean (or in situ deposited) SN interfaces. The resistance of the junctions is dominated by this contact resistance.

Besides increasing the resistance of the junctions, the ${\rm SrTiO_3}$ layer increases the capacitance of the junctions. Hysteretic I-V characteristics were observed from 4.2 K up to 80 K in the type B junctions. From the curve shown in Fig. 2(b), we can estimate the McCumber parameter, $\beta_c = 2{\rm eI}_c {\rm R}_n^2 C/\hbar$, to be about 20. For this junction, this corresponds to a capacitance of 40 pF. This is the value of capacitance we expect for the parallel plate capacitor formed by the 100 nm ${\rm SrTiO_3}$ layer between the YBCO and Au layers. The ${\rm SrTiO_3}$ has a resistivity above $10^4~\Omega$ -cm and a relative dielectric constant of about 50.

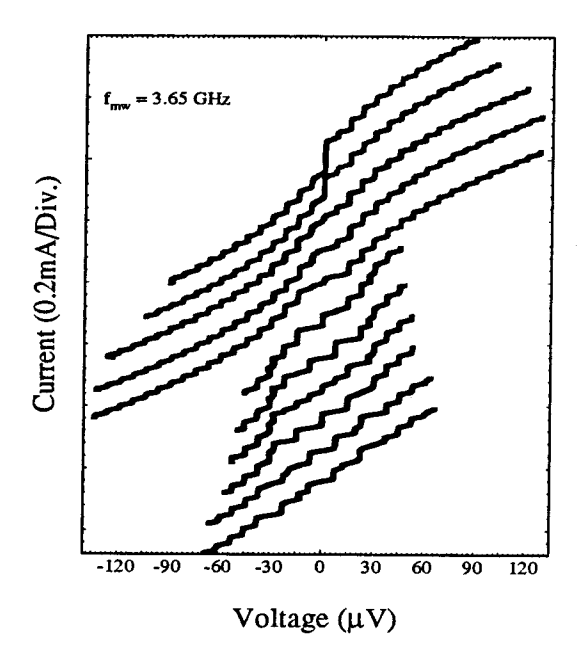


Fig. 3. Clear Shapiro steps are observed at temperatures from 4.2 K to 85 K. These curves are measured on a type A junction at 4.2 K. The different curves are different power levels.

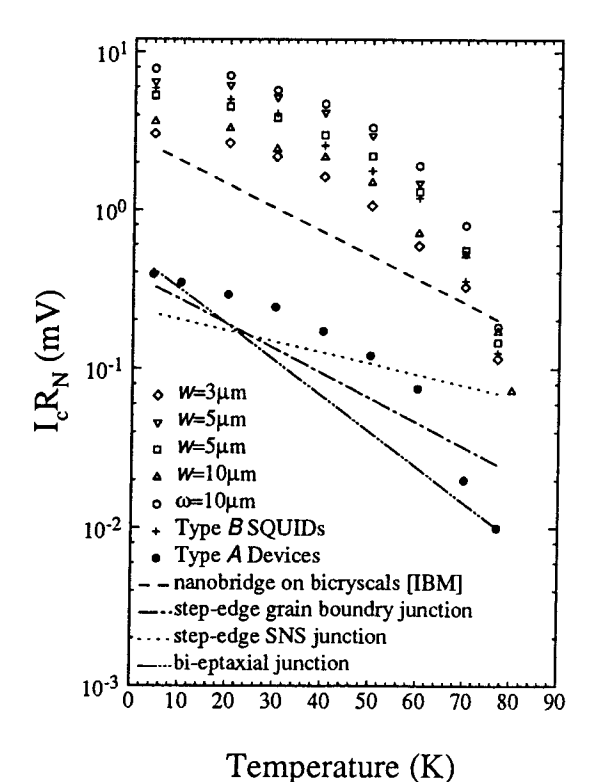


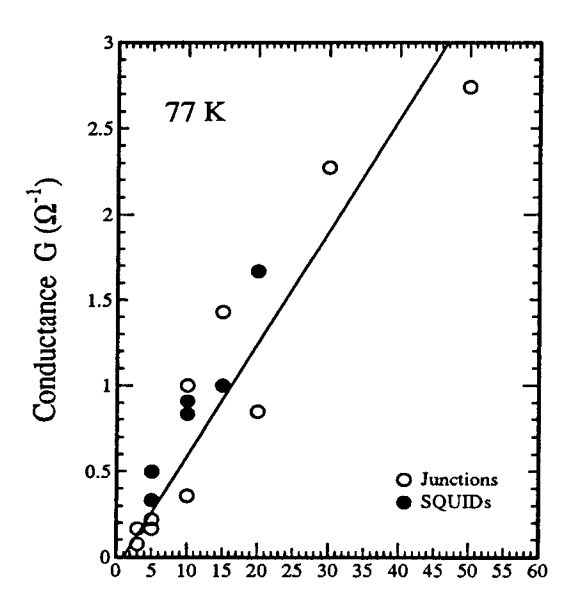
Fig. 4. The I_cR_n product as a function of temperature for different kinds of junctions. All the open data are for type B devices with different widths w. The solid data is the average value for the type A devices.

Figure 3 shows a typical I-V characteristic of the junctions in the presence of about 4 GHz microwave irradiation with different power levels. Clear Shapiro steps were observed at temperatures up to 85 K. In Fig. 4, the I_cR_n values for several kinds of junctions are plotted as a function of temperature. Our type A junctions have a I_cR_n product of 0.01 mV at 77 K and 0.4 mV at 4.2 K while the type B junctions have I_cR_n products of 0.18 mV at 77 K and 7.8 mV at 4.2 K. For comparison the temperature dependence of the I_cR_n product the step edge grain boundary junctions, biepitaxial junctions, and bicrystal substrate junctions are included in the figure.

Figure 5 shows the conductance of type B junctions and SQUIDs at 77 K versus junction width (and hence area). This demonstrates that the conductance scales with area. The conductance plotted here is the asymptotic value taken at high voltage from the I-V characteristics. For both type A and type B junctions the conductance is temperature independent. The typical magnetic diffraction pattern shown in Fig. 6. The nodes in the critical current occur every 4.3 G. This agrees with the calculated value of $H_p = \Phi_0/\mu_0 A_{eff}$, where the effective area is $A_{eff} \sim (2\lambda_L + h)w$. Here h is the step height, w is the width of the junction, and λ_L is the London penetration depth, $\lambda_L \sim 250$ nm at 77 K.

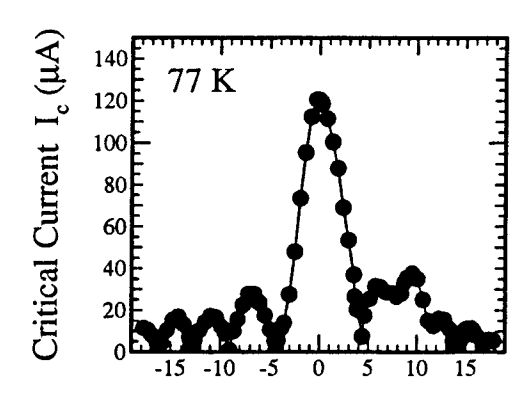
4. dc-SQUIDs

The dc-SQUIDs were made using both type A or nonhysteretic type B junctions. The SQUIDs are composed of two 5-, 10-, 15- or 20-µm-wide junctions with SQUID loop areas of either 100 or 300 μm². The voltage modulation peak to peak (V_{pp}) with applied magnetic field at 77 K was about 1-2 μV for an type A SQUIDs and about 3-10 μ V for an type B SOUIDs. Figure 7 shows flux noise spectra taken at 77 K for both types of SQUIDs. The noise measurements are performed in an open loop mode and the SOUIDs are coupled to a low noise FET amplifier by means of a room-temperature matching transformer. The total gain we used was 5×10⁶ and the resolution of measuring system was $0.04 \text{ nV}/\sqrt{Hz}$. The voltage noise spectral density $S_v^{1/2}$ is about 0.6 nV/ \sqrt{Hz} at 77 K for both type A and type B SQUIDs. The flux noise spectral density, $S_{\phi}^{1/2}$, is given by $S_{\phi}^{1/2} = S_{\nu}^{1/2}/(\delta V/\delta \Phi)$. For the type B SQUIDs the flux noise is lower than that of type A SQUIDs because of large flux-voltage conversion. The minimum flux noise spectral density, is about $80 \,\mu\Phi_0/\sqrt{Hz}$ for a type A SQUIDs, and $30 \,\mu\Phi_0/\sqrt{Hz}$ for a type B SQUIDs. The knee of 1/f noise is between one and a few Hz. This is one of



Junction Width $W(\mu m) \propto Area$

Fig. 5. Conductance (G) vs junction width for type B devices on a single chip at 77 K. There is a nearly linear scaling relationship between the G and area.



Applied Magnetic Field H (G)

Fig. 6. A typical magnetic diffraction pattern measured in liquid nitrogen for one of type B junctions. The magnetic field normal to the substrate plane was applied by a solenoid above the sample.

the lowest noise figures reported at 1 Hz for a 77 K SQUIDs and is comparable to the results obtained from a commercial niobium dc-SQUIDs at 4.2 K. Better results at higher frequencies have been obtained by Ramos et al.8 on step-edge grain boundary junctions ($\sim 3 \mu \Phi_o / \sqrt{Hz}$ at 100 Hz) and by Kawasaki et al.9 on nanobridge bicrystal junctions ($\sim 3 \mu \Phi_o / \sqrt{Hz}$ at 71 kHz). Finally, we estimate the energy resolution for our SQUIDs. Theoretically, one expects the energy resolu-

tion to be $\varepsilon = 9k_BTL/R_n \approx 4 \times 10^{-31} \text{ J/Hz}$, where the inductance of SQUIDs, L, was estimated to be about 80 pH. ¹⁰ The experimental energy resolution for the type B SQUIDs was $S_{\phi}/2L = 2.4 \times 10^{-29} \text{ J/Hz}$. For this SQUID, $\beta_L = 2LI_c/\Phi_0 \approx 1.5$.

5. Hysteretic Junctions for High-T, ROS

Relaxation oscillation SQUIDs (ROS) utilize a flux to frequency readout rather than the flux to voltage readout used in conventional dc-SQUIDs. II This readout scheme greatly simplifies the readout electronics. Although ROS devices are being developed using low- T_c superconductors, the fabrication of ROS using high- T_c materials has been prevented by the lack of underdamped high- T_c junctions.

In addition to the reduced the shunt conductance, the type B junctions have an increased shunt capacitance. Both of these factors increase the McCumber parameter, β_c , and allow for the fabrication of underdamped junctions. The gate area and the thickness of the dielectric $SrTiO_3$ can be modified to control the hysteretic behavior. Thermal noise can suppress the hysteresis in underdamped junctions. Simulations based on the RSCJ model indicate for a noise parameter of $\gamma = 100$, the hysteresis is greatest for β_c in the range 10-80. This is consistent with the experiments where the best hysteretic behavior occurs at $\beta_c \approx 20$.

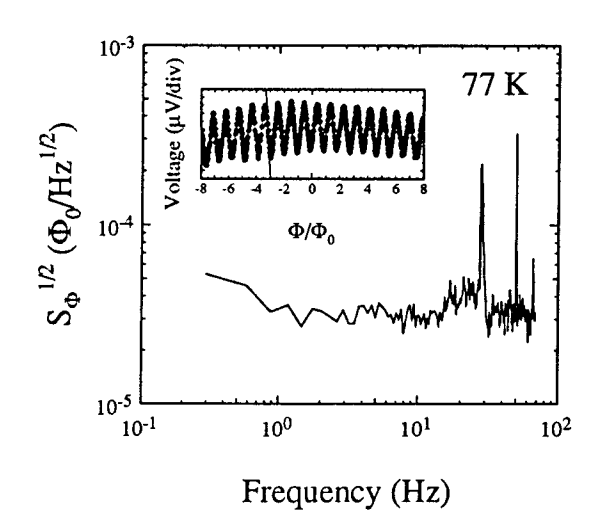


Fig. 7. Equivalent flux noise spectrum as a function of frequency for a nonhysteretic type B dc-SQUID. The SQUID is operated in an open loop mode in liquid nitrogen. One of the best voltage-flux modulations is shown in the inset which indicates $V_{pp} \sim 7 \,\mu\text{V}$ and $\delta\text{V}/\delta\Phi \sim 21 \,\mu\text{V}/\Phi_0$.

6. Conclusions

We have fabricated and measured YBCO/Au/YBCO step-edge SNS junctions and dc-SQUIDs using an all in situ laser ablation deposition. The I_cR_n products of the junctions were 0.18 mV at 77 K and 7.83 mV at 4.2 K. These large I_cR_n products were made possibly by depositing an insulating layer between YBCO and Au electrodes. This extra process minimizes the shunt conductance without reducing the Josephson supercurrent. The best dc-SQUID made from these junctions had a flux noise spectral density in the range of $30 \, \mu \Phi_o / \sqrt{Hz}$ and the knee of 1/f noise was at about 1 Hz.

7. References

and 2177 (1991).

- [1] M. S. DiIorio, S. Yoshizumi, K-Y Yang, J. Zhang, and M. Maung, Appl. Phys. Lett. 58, 2552 (1991); M. S. DiIorio, S. Yoshizumi, M. Maung, K-Y Yang, J. Zhang, and N. Q. Fan, Nature 354, 513 (1991).
- [2] R. Wunderlich, C. Francke, J. Langer, B. Meyer, and J. Müller, EUCAS'93, Oct. 4-8, 1993, Göttingen, Germany, "Applied Superconductivity" Editor H. C. Freyhardt, Vol. 2, p. 1351.
- [3] Z. W. Dong, P. Hadley, and J. E. Mooij, Proceedings of the 4th International Superconductive Electronics Conference, p.219, Colorado, USA, August 11-14, 1993; Z. W. Dong, P. Hadley, and J. E. Mooij, ECAUS'93, Göttingen, Germany, October 4-8, 1993, "Applied Superconductivity", Editor H. C. Freyhardt, Vol. 2, p.1215.
- [4] J. W. Ekin, S. E. Russek, C. C. Clickner, and B. Jeanneret, Appl. Phys. Lett. **62**, 369 (1993).
- [5] G. Friedl, M. Vildic, B. Roas, D. Uhl, F. Bömmel, M. Römheld, B. Hillenbrand, B. Stritzker, and G. Daalmans, Appl. Phys. Lett. 60, 3048 (1992); H. Kohlstedt, J. Schubert, K. Herrmann, M. Siegel, C. A. Copetti, W. Zander and A. I. Braginski, Supercond. Sci. Technol. 6, 246 (1993); D. Grundler, R. Eckart, B. David and O. Dosel, Appl. Phys. Lett. 62, 2134 (1993). [6] K. Char, M. S. Colclough, S. M. Garrison, N. Newman, and G. Zaharchuk, Appl. Phys. Lett. 59, 733
- [7] R. Gross and B. Mayer, Physica C 180, 235 (1991);
 B. Mayer, S. Schuster, A. Beck, L. Alff, and R. Gross, Appl. Phys. Lett. 62, 783 (1993).
- [8] J. Ramos, T. Claeson, Z. Ivanov, G. Daalmans, D. Uhl, F. Bömmel, EUCAS'93, Oct. 4-8, 1993, Göttingen, Germany, "Applied Superconductivity" Editor H. C. Freyhardt, Vol. 2, p. 1371.
- [9] M. Kawasaki, P. Chaudhari, T. H. Newman, and A. Gupta, Appl. Phys. Lett. **58**, 2555 (1991).
- [10] J. Clarke, "SQUID Concepts and Systems", NATO ASI Series, Vol. F59, 98 (1989); J. M. Jaycox and M.

B. Ketchen, IEEE Tans. Magn. MAG-17, 400 (1981); W. H. Chang, IEEE Tans. Magn. MAG-17, 764(1981). [11] F. L. Vernon and R. J. Pederson, J. Appl. Phys. 39, 2661 (1968); M. Mück, H. Rogalla and C. Heiden, Appl. Phys. A 47, 285 (1988); G. Uehara, T. Morooka, J. Kawai, N. Mizutani and H. Kado, IEEE Trans. Appl. Supercond. 3, 1866 (1993).